Hindawi
Journal of Nanomaterials
Volume 2019, Article ID 6862390, 11 pages
https://doi.org/10.1155/2019/6862390

Research Article

Quantitative Phase-Field Simulation of Composition Partition and Separation Kinetics of Nanoscale Phase in Fe-Cr-Al Alloy

Shi Chen,[1,2] Yongsheng Li,[1,2] Shujing Shi,[1,2] and Shengshun Jin[1,2]

[1]*School of Materials Science and Engineering, Nanjing University of Science and Technology, Nanjing 210094, China*
[2]*MIIT Key Laboratory of Advanced Metallic and Intermetallic Materials Technology, Nanjing 210094, China*

Correspondence should be addressed to Yongsheng Li; ysli@njust.edu.cn

Received 3 January 2019; Accepted 4 April 2019; Published 8 May 2019

Academic Editor: Jean M. Greneche

Phase separation of the Cr-enriched nanoscale α' phase in the Fe-38 at.% Cr-10 at.% Al alloy is studied by utilizing phase-field simulation. The partition of elements in the α and α' phases is clarified with the composition evolution through the α/α' phase interface, and the separation kinetics is quantitatively investigated by the temporal evolution of the size and volume fraction of the α' phase. Aluminum partitions into the Fe-enriched α phase and depletes in the α' phase, and the partition coefficient decreases as the temperature changes from 720 K to 760 K for the steady-state coarsening stage. As the temperature increases, the initial change rate of the volume fraction of the α' phase is faster, indicating an accelerated phase separation. At the coarsening stage, the average particle distance and coarsening rate constant of the α' phase increase with increased temperature, and the ratio of the Ostwald ripening is dominating compared with coalescence coarsening. The element partition and kinetics evolution of the α' phase with temperature are helpful for the morphology and property predication of nanoscale precipitates.

1. Introduction

Fe-Cr-Al alloys have good corrosion resistance, radiation resistance, and mechanical strength, and they are being developed as structural materials for the next generation of nuclear reactors, such as fusion reactors, sodium fast reactors, lead-cooled fast reactors, and supercritical water reactors [1–5]. Also, because of the comprehensive performance of Fe-Cr-Al alloys in steam environments, these alloys are under consideration for accident-tolerant fuel-cladding applications [6–8].

However, when the Cr concentration in Fe-Cr-based alloys is greater than 15 at.% and alloys are heated or slowly cooled at 300-500°C, embrittlement of the alloys will increase, which is harmful to the mechanical properties. The embrittlement is caused by the decomposition of the ferrite phase into Fe-enriched α and Cr-enriched α' phases in Fe-Cr-based alloys [9–11]. The separation of the nanoscale α' phase can happen via spinodal decomposition or nucleation and growth, which depends on the concentration of Cr and the aging temperature of the alloys [12, 13]. However, studies show that additional Al (≥2.5 at.%) provides a benefit in suppressing the α' phase separation [14, 15].

In the past few decades, more attention has been paid to Fe-Cr binary alloys to understand phase decomposition by experiments and computer simulations [16–21]. As a new potential alloy in nuclear plants, Fe-Cr-Al alloys attracted much attention and were studied by utilizing the computer coupling of phase diagrams and thermochemistry formulation. For example, the miscibility gap of the PM 2000™ ODS alloy (Fe-20 at.% Cr-10 at.% Al) was studied by Capdevila et al. [22]. Comparing with the Fe-20 at.% Cr alloy, the critical temperature is reduced and the miscibility gap is narrowed. Composition difference was found to increase by approximately following the time exponent of 1/3 for aging to 3600 h. Also, they observed that Al partitions preferentially into the α phase rather than the α' phase. Kobayashi and Takasugi studied the effect of Al on the embrittlement of Fe-(10-30) at.% Cr-(0-20) at.% Al alloys [15]. The results showed that embrittlement will be induced when the concentration of Al is less than 2 at.%, while a large amount of Al restrains embrittlement. In addition, the effect of Al on the

formation energies and interfacial energy was studied by using the first-principles theory [23]. It showed that the suppression of embrittlement by adding Al in Fe-Cr alloys could be attributed to the effect of Al on the formation energies rather than on the interfacial energy. Ejenstam et al. found that the Fe-21 wt.% Cr-5 wt.% Al alloy is readily embrittled at 475 and 500°C rather than at 550°C. Furthermore, the tendency of Cr clustering is more obvious with the atom probe tomography (APT) analysis when the alloy is aged at the lower temperature [3]. In addition, the effects of other elements on the phase separation in Fe-Cr alloys were studied. Suwa et al. studied the effect of Mo on phase separation in the Fe-40 at.% Cr alloy with numerical simulation based on the Cahn-Hilliard equation [24, 25]. Lv et al. studied the microstructure evolution in Fe-Cr-Co alloys during thermal magnetic treatment and step aging with phase-field simulation [26].

However, the quantitative separation kinetics of the nanoscale α' phase and composition partition in Fe-Cr-Al alloys are not clearly studied, which are important for the morphology evolution of long aging time and predication of the mechanical properties of these alloys. The volume fraction and average particle radius of the α' phase will be changed with the composition and temperature change, and the morphology of the α' phase affects the hardness and embrittlement directly in Fe-Cr-Al alloys, so the evolution kinetics combined with the change of mechanical properties will be helpful in predicating the longtime variation of the functional properties of Fe-Cr-Al alloys. In this work, we investigate the composition partitions in the α and α' phases and the evolution kinetics of the α' phase in the Fe-38 at.% Cr-10 at.% Al alloy aged at 720, 740, and 760 K by utilizing phase-field simulation [27]. The selected temperatures are located in the region of spinodal decomposition [22], and the effect of aging temperature on the separation behavior of the nanoscale phase in the ternary Fe-Cr-Al alloy will be clarified.

2. Model and Methods

2.1. Phase-Field Model. The microstructure evolution of the Cr-enriched α' phase in Fe-Cr-Al alloys can be described by the composition evolution of Cr and Al with the composition conservation condition $c_{\mathrm{Fe}} = 1 - c_{\mathrm{Cr}} - c_{\mathrm{Al}}$, which is controlled by the Cahn-Hilliard nonlinear diffusion equation [28]:

$$\begin{aligned}\frac{\partial c_{\mathrm{Cr}}(\mathbf{r},t)}{\partial t} &= V_{\mathrm{m}}\nabla\left(M_{\mathrm{Cr,Cr}}\nabla\frac{\delta F}{\delta c_{\mathrm{Cr}}} + M_{\mathrm{Cr,Al}}\nabla\frac{\delta F}{\delta c_{\mathrm{Al}}}\right),\\ \frac{\partial c_{\mathrm{Al}}(\mathbf{r},t)}{\partial t} &= V_{\mathrm{m}}\nabla\left(M_{\mathrm{Al,Cr}}\nabla\frac{\delta F}{\delta c_{\mathrm{Cr}}} + M_{\mathrm{Al,Al}}\nabla\frac{\delta F}{\delta c_{\mathrm{Al}}}\right),\end{aligned} \tag{1}$$

where c_{Cr} and c_{Al} are the nominal compositions of Cr and Al, respectively, V_{m} is the molar volume of the alloy, and $\mathbf{r} = (\mathbf{r_1}, \mathbf{r_2}, \mathbf{r_3})$ and t are the spatial coordinates and time, respectively.

M_{ij} is the Onsager coefficient and determined by the atomic mobility [29–31]:

$$\begin{aligned}M_{\mathrm{Cr,Cr}} &= \left[c_{\mathrm{Fe}}c_{\mathrm{Cr}}M_{\mathrm{Fe}} + (1-c_{\mathrm{Cr}})^2 M_{\mathrm{Cr}} + c_{\mathrm{Cr}}c_{\mathrm{Al}}M_{\mathrm{Al}}\right]c_{\mathrm{Cr}},\\ M_{\mathrm{Al,Al}} &= \left[c_{\mathrm{Fe}}c_{\mathrm{Al}}M_{\mathrm{Fe}} + c_{\mathrm{Cr}}c_{\mathrm{Al}}M_{\mathrm{Cr}} + (1-c_{\mathrm{Al}})^2 M_{\mathrm{Al}}\right]c_{\mathrm{Al}},\\ M_{\mathrm{Cr,Al}} &= M_{\mathrm{Al,Cr}} = \left[c_{\mathrm{Fe}}M_{\mathrm{Fe}} - (1-c_{\mathrm{Cr}})M_{\mathrm{Cr}} - (1-c_{\mathrm{Al}})M_{\mathrm{Al}}\right]c_{\mathrm{Cr}}c_{\mathrm{Al}},\end{aligned} \tag{2}$$

where M_{Fe}, M_{Cr}, and M_{Al} are the atomic mobilities of Fe, Cr, and Al, respectively. They are expressed by $M_i = D_i/RT$, where i denotes the element Fe, Cr, or Al, R is the gas constant, T is the absolute temperature, and D_i is the diffusion coefficient and chosen as [32–35] $D_{\mathrm{Fe}} = 1.0 \times 10^{-4} \exp(-294\,\mathrm{kJ\,mol^{-1}}/RT)$, $D_{\mathrm{Cr}} = 2.0 \times 10^{-5} \exp(-308\,\mathrm{kJ\,mol^{-1}}/RT)$, and $D_{\mathrm{Al}} = 1.1 \times 10^{-4} \exp(-218\,\mathrm{kJ\,mol^{-1}}/RT)$.

The total free energy F of Fe-Cr-Al alloys includes the Gibbs energy and interfacial energy. For the small lattice mismatch between the α and α' phases, the elastic strain energy is ignored. The free energy is expressed as [36, 37]

$$F = \int_V \left\{\frac{1}{V_{\mathrm{m}}}\left[G + \kappa_{\mathrm{Fe}}(\nabla c_{\mathrm{Fe}})^2 + \kappa_{\mathrm{Cr}}(\nabla c_{\mathrm{Cr}})^2 + \kappa_{\mathrm{Al}}(\nabla c_{\mathrm{Al}})^2\right]\right\} dV, \tag{3}$$

where κ_{Fe}, κ_{Cr}, and κ_{Al} are the gradient energy coefficient of Fe, Cr, and Al, respectively. G is the molar Gibbs energy and written as [38, 39]

$$\begin{aligned}G = {} & c_{\mathrm{Fe}}G^0_{\mathrm{Fe}} + c_{\mathrm{Cr}}G^0_{\mathrm{Cr}} + c_{\mathrm{Al}}G^0_{\mathrm{Al}} + L_{\mathrm{FeCr}}c_{\mathrm{Fe}}c_{\mathrm{Cr}}\\ & + L_{\mathrm{FeAl}}c_{\mathrm{Fe}}c_{\mathrm{Al}} + L_{\mathrm{CrAl}}c_{\mathrm{Cr}}c_{\mathrm{Al}}\\ & + RT(c_{\mathrm{Fe}}\ln c_{\mathrm{Fe}} + c_{\mathrm{Cr}}\ln c_{\mathrm{Cr}} + c_{\mathrm{Al}}\ln c_{\mathrm{Al}}) + G_{\mathrm{m}},\end{aligned} \tag{4}$$

where G^0_{Fe}, G^0_{Cr}, and G^0_{Al} are the molar Gibbs free energy of pure Fe, Cr, and Al, and their expressions are given by [40]. L_{ij} is the interaction parameter between elements i and j, and it is given by $L_{\mathrm{FeCr}} = 20500 - 9.68T$, $L_{\mathrm{FeAl}} = -122452.9 + 31.6455T$, and $L_{\mathrm{CrAl}} = -54900 + 10T$ [41, 42]. G_{m} is the magnetic ordering contribution to the Gibbs energy, which is expressed by $G_{\mathrm{m}} = RT\ln(\beta+1)f(\tau)$ [41–43], where β is the atomic magnetic moment and expressed by $\beta = 2.22c_{\mathrm{Fe}} - 0.008c_{\mathrm{Cr}} - 0.85c_{\mathrm{Fe}}c_{\mathrm{Cr}}$. The function $f(\tau)$ is referred in the literature [41–43].

For simplicity, the gradient coefficients κ_{Fe}, κ_{Cr}, and κ_{Al} are assumed the same, $\kappa_{\mathrm{Fe}} = \kappa_{\mathrm{Cr}} = \kappa_{\mathrm{Al}} = 1/6r_0^2 L_{\mathrm{FeCr}}$, where r_0 is the interatomic distance at the stress-free state and changes with composition by obeying Vergard's law [32]. It should be noted that the composition effects are neglected in the gradient coefficient, which may have an influence on the interface width [28, 44].

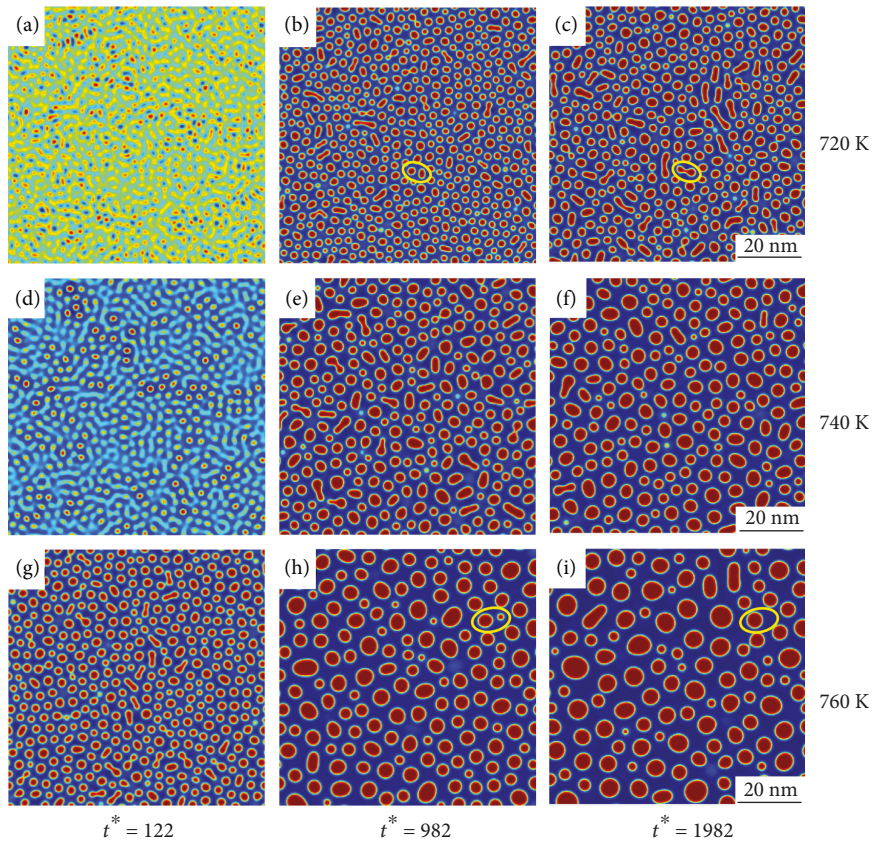

Figure 1: Morphology evolution of the α' phase in the Fe-38 at.% Cr-10 at.% Al alloy aged at 720, 740, and 760 K.

2.2. Numerical Methods. By transforming equations into the dimensionless form for the numerical calculation, we have

$$\begin{aligned}\frac{\partial c_{\mathrm{Cr}}(\mathbf{r}^*,t^*)}{\partial t^*} &= \nabla^*\left[M^*_{\mathrm{Cr,Cr}}\nabla^*\left(\frac{\partial G^*}{\partial c_{\mathrm{Cr}}} - 4\kappa^*_{\mathrm{c}}(\nabla^*)^2 c_{\mathrm{Cr}}\right.\right.\\ &\quad \left. - 2\kappa^*_{\mathrm{c}}(\nabla^*)^2 c_{\mathrm{Al}}\right) + M^*_{\mathrm{Cr,Al}}\nabla^*\left(\frac{\partial G^*}{\partial c_{\mathrm{Al}}}\right.\\ &\quad \left.\left. - 4\kappa^*_{\mathrm{c}}(\nabla^*)^2 c_{\mathrm{Al}} - 2\kappa^*_{\mathrm{c}}(\nabla^*)^2 c_{\mathrm{Cr}}\right)\right],\\ \frac{\partial c_{\mathrm{Al}}(\mathbf{r}^*,t^*)}{\partial t^*} &= \nabla^*\left[M^*_{\mathrm{Al,Cr}}\nabla^*\left(\frac{\partial G^*}{\partial c_{\mathrm{Cr}}} - 4\kappa^*_{\mathrm{c}}(\nabla^*)^2 c_{\mathrm{Cr}}\right.\right.\\ &\quad \left. - 2\kappa^*_{\mathrm{c}}(\nabla^*)^2 c_{\mathrm{Al}}\right) + M^*_{\mathrm{Al,Al}}\nabla^*\left(\frac{\partial G^*}{\partial c_{\mathrm{Al}}},\right.\\ &\quad \left.\left. - 4\kappa^*_{\mathrm{c}}(\nabla^*)^2 c_{\mathrm{Al}} - 2\kappa^*_{\mathrm{c}}(\nabla^*)^2 c_{\mathrm{Cr}}\right)\right]\end{aligned} \tag{5}$$

where $\mathbf{r}^* = \mathbf{r}/l$, $t^* = tD/l^2$, $M^*_{ij} = RT_0M_{ij}/D$, $G^* = G/RT_0$, $\kappa^*_{\mathrm{c}} = \kappa_{\mathrm{c}}/RT_0l^2$, l is the grid length and chosen as the average lattice constant a_0, $a_0 = a_{\mathrm{Fe}}c_{\mathrm{Fe}} + a_{\mathrm{Cr}}c_{\mathrm{Cr}} + a_{\mathrm{Al}}c_{\mathrm{Al}}$, and the lattice parameters are $a_{\mathrm{Fe}} = 2.866 \times 10^{-10}$ m, $a_{\mathrm{Cr}} = 2.882 \times 10^{-10}$ m, and $a_{\mathrm{Al}} = 4.050 \times 10^{-10}$ m [45]. The lattice parameters will be affected by composition and temperatures, while the lattice mismatch in the alloy is small enough; we assume the lattice parameters as constants. $D = 10^{-25}$ $\mathrm{m^2s^{-1}}$ is adopted as the normalization factor. $T_0 = 875$ K is the critical temperature of phase separation of the Fe-38 at.% Cr-10 at.% Al alloy. The grid size is chosen as $\Delta x = \Delta y = l$; thus, the dimensionless grid size is 1.0, which is convenient for calculating. The grid number of the simulation cell is 256×256, and the dimensionless time step is 0.001 for insuring the accuracy in solving the partial differential equation. To induce the phase separation, a random thermal fluctuation with magnitude $[-0.002, 0.002]$ was introduced into the initial composition. It should be noted that the thermal fluctuation should have a minimum magnitude for triggering the phase separation, as a large fluctuation may affect the initial particle number and particles' radii. The semi-implicit Fourier spectral method was adopted to solve the Cahn-Hilliard equation with a variable coefficient [46].

3. Results and Discussion

3.1. Morphology and Composition Evolution of α' Phase. Figure 1 shows the morphology evolution of the Cr-enriched α' phase in the Fe-38 at.% Cr-10 at.% Al alloy aged at 720, 740, and 760 K, where the blue regions represent the Fe-enriched α phase and the red regions represent the Cr-enriched α' phase. It can be seen from Figures 1(a), 1(d), and 1(g) that the separated α' phase becomes obvious and the particle number increases with increasing temperature. For the aging temperature of 740 K, there are some separated

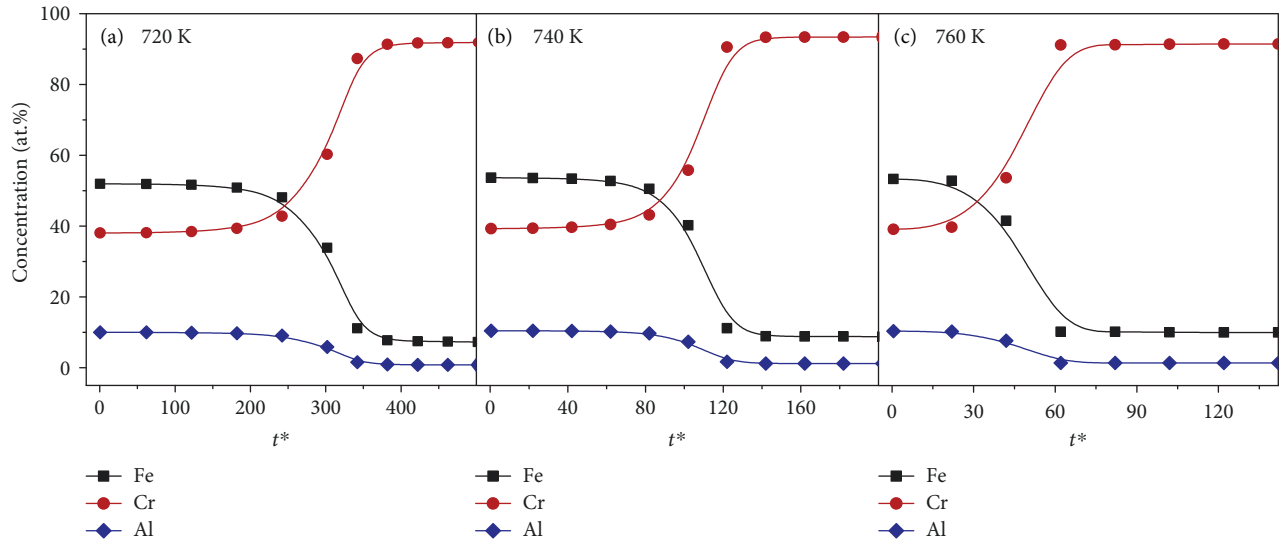

Figure 2: Variations of the composition in the α' phase as a function of time in the Fe-38 at.% Cr-10 at.% Al alloy aged at 720, 740, and 760 K.

α' phases (Figure 1(d)). At the same time, only composition clustering can be observed in Figure 1(a), while the α' phase has separated completely at 760 K (Figure 1(g)). This is because the difference of free energy between the α phase and the α' phase increases with increased temperature, which leads to the accelerated phase separation. In addition, the particle size of the α' phase is larger at 760 K than that of the other temperatures for the same aging time. From Figures 1(b) and 1(c), it can be found that coalescence coarsening of some α' phases happens via the interconnection of neighboring particles and forms a worm shape or elliptical shape, such as the particles in the circles. However, as the temperature increases, the particles' distance is enlarged and the Ostwald ripening becomes obvious, as shown in the two particles labelled with circles in Figures 1(h) and 1(i).

Capdevila et al. showed, using APT, that the isoconcentration surfaces of the α' phases are isolated in the Fe-20 at.% Cr-10 at.% Al alloy aged at 748 K for 3600 h, while at the lower temperature of 673 K, an interconnected network of the Cr-enriched phase is observed [22, 47]. Because the α' phase is shown in the two-dimensional morphology and the temperature is not low enough, the interconnected network is not observed; however, for the three-dimensional morphology in the Fe-35 at.% alloy aged at 700-750 K, an interconnected network of the α' phase is observed [48]. Kobayashi and Takasugi observed spherical-like particles in the Fe-17 at.% Cr-8 at.% Al alloy [15]. In addition, the separated particles and the worm shaped α' phase are similar to the high resolution transmission electron microscopy (HR-TEM) micrographs of the Fe-40 at.% Cr alloy aged at 773 K for 750 h [49, 50]. Therefore, the simulated morphology of the α' phase in the Fe-38 at.% Cr-10 at.% Al alloy is reasonable.

Figure 2 shows the evolution of the composition in the α' phase as a function of time for the Fe-38 at.% Cr-10 at.% Al alloy at 720, 740, and 760 K. It can be clearly seen that as aging goes on, the concentrations of Fe and Al decrease from the initial nominal compositions of 52 at.% and 10 at.% to about 8 at.% and 1 at.% in the α' phase at the three temperatures, while the Cr concentration increases from 38 at.% to about 90 at.% in the α' phase. The concentrations of the elements begin to change from the initial average values to the composition of the α' phase at $t^* = 242$, 82, and 22 for the aging temperatures of 720, 740, and 760 K, respectively, as shown by the crossover points of Cr and Fe in Figures 2(a), 2(b), and 2(c). The results indicate that the change of composition in the α' phase is faster with the increased aging temperature, which is similar to Capdevila's APT results [22].

Table 1: Composition variations of the α' phase for the different aging temperatures and times.

T (K)	t^*	α' composition (at.%)			$C\alpha_{Al}/C\alpha'_{Al}$
		Fe	Cr	Al	
720	0.5	51.92	38.07	10.01	1.00
	282	41.79	50.59	7.62	1.45
	322	20.37	76.49	3.14	3.87
	402	7.49	91.66	0.85	17.36
	1982	6.90	92.30	0.80	18.88
740	0.5	51.97	38.03	10.00	1.00
	102	38.94	54.06	7.00	1.54
	122	10.69	87.79	1.52	8.36
	142	8.48	90.48	1.04	13.97
	1982	8.16	90.87	0.97	14.83
760	0.5	51.96	38.05	9.99	1.00
	42	40.41	52.25	7.34	1.50
	62	9.85	88.89	1.26	11.44
	1982	9.50	89.27	1.23	11.76

Table 1 shows the composition values of Fe, Cr, and Al in the α' phase for the Fe-38 at.% Cr-10 at.% Al alloy aged at

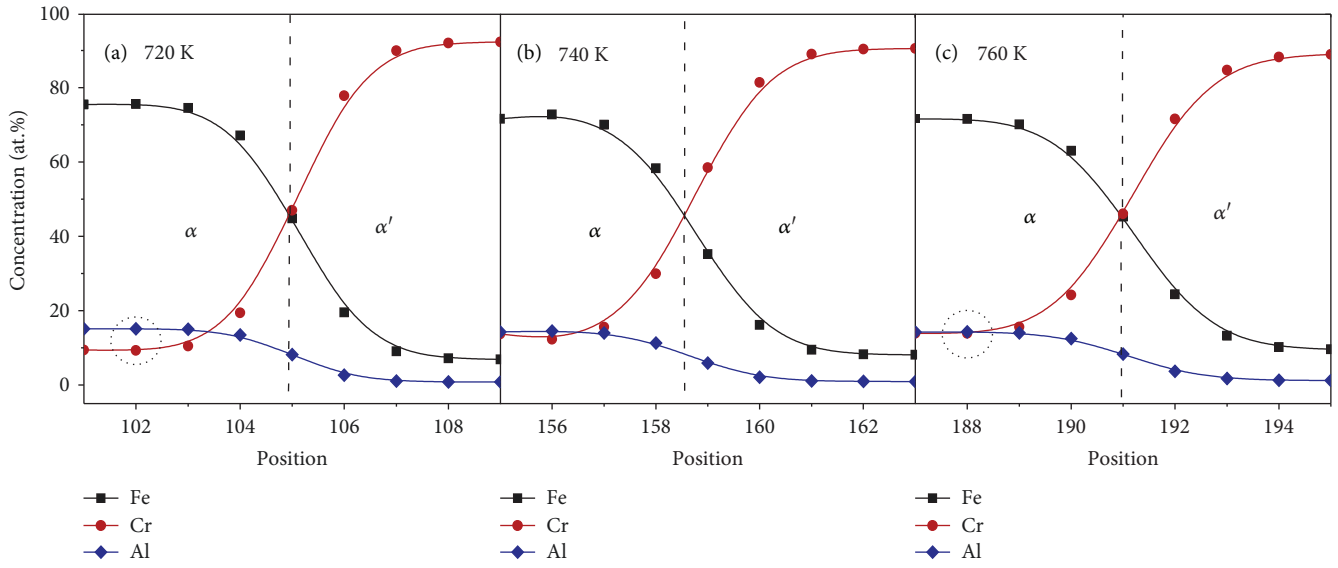

FIGURE 3: The concentration distributions of Fe, Cr, and Al through the interface of the α/α' phase in the Fe-38 at.% Cr-10 at.% Al alloy aged at 720, 740, and 760 K for $t^* = 1982$.

different times and temperatures. We define the equilibrium composition of the α' phase with $(c_{t_1} - c_t)/c_t \leq 1.0\%$, where c_t and c_{t_1} denote the compositions at a time and at a long enough time, respectively. If the composition difference between the two times is less than 1.0%, the composition c_t can be regarded as the equilibrium composition. Therefore, the equilibrium compositions of the α' phase are reached at $t^* = 402$, 142, and 62 for 720, 740, and 760 K, respectively, as can be seen in Figure 2. It indicates that the α' phase reaches the equilibrium composition earlier with increased aging temperature. The APT results also showed that the equilibrium composition of the α' phase is reached earlier with the temperature increasing [22].

The equilibrium concentrations of Cr in the α' phase at 720, 740, and 760 K are 91.7 at.%, 90.5 at.%, and 88.9 at.%, respectively. The equilibrium concentrations of Fe and Al in the α' phase are 7.49 at.% and 0.85 at.% at 720 K, 8.48 at.% and 1.04 at.% at 740 K, and 9.85 at.% and 1.26 at.% at 760 K, respectively. Read and Hono calculated that the equilibrium Cr concentration is 91.3 at.% in the α' phase for the Fe-20.2 at.% Cr-8.8 at.% Al alloy aged at 748 K [51]. For the Fe-20 at.% Cr-10 at.% Al alloy aged at 708 K for 3600 h, the Cr concentration in the α' phase is 84.8 at.% [52]. The partition coefficients of Al in the α and α' phases, $C\alpha_{Al}/C\alpha'_{Al}$, were calculated, as shown in Table 1. It was found that Al strongly partitions into the α phase with increased aging time. There is no doubt that the equilibrium concentration of the α' phase can be given in the thermodynamic phase diagram; however, the concentration and morphology evolution of the α' phase cannot be shown by the thermodynamic calculation, which is why the phase-field simulation is attractive for studying the temporal morphology and composition evolution.

In order to study the elements' partitioning in the α and α' phases, Figure 3 displays the concentration distributions of Fe, Cr, and Al across the interface of the α/α' phase in the Fe-38 at.% Cr-10 at.% Al alloy aged at 720, 740, and 760 K for $t^* = 1982$. At this time, the composition of the α' phase has reached the equilibrium values, as shown in Table 1. The concentration is calculated from $x^* = 101$ to 109, 155 to 163, and 187 to 195 for 720, 740, and 760 K, respectively. It can be seen that Al depletes in the Cr-enriched α' phase, i.e., Al strongly partitions into the Fe-enriched α phase. Previous studies demonstrated that if there is a sufficient chemical potential gradient, the partitioning of Al will begin [53]. It is thought that at the early stage of phase separation, the composition difference between the α phase and the α' phase is small and the difference of the Al chemical potential in the two phases is likewise small, which is why Al does not show a clear partition. After a long aging time, the chemical potentials of Al in the two phases have a sufficient difference due to the composition difference and the partition of Al into the α phase happens [47, 53, 54], which can also be distinguished in Figure 2. Capdevila et al. found the partitioning of Al into the α phase by utilizing APT [55]. In the α phase, the concentration of Al is higher than Cr at 720 K, and the Al concentration has almost no change as the temperature increases to 760 K, which is similar with the increased Cr concentration at 760 K as indicated by the dotted circles in Figures 3(a) and 3(c). The results show that the partitioning of Al into the α phase has no obvious change as the temperature increases, while the partitioning of Cr into the α phase is enhanced. Furthermore, the concentration of Fe in the α phase decreases as the aging temperature increases.

3.2. Phase Separation Kinetics of α' Phase. The variations of the volume fraction of the α' phase as a function of time in the Fe-38 at.% Cr-10 at.% Al alloy aged at different temperatures are shown in Figure 4. It is obvious that the volume fraction is near zero at the beginning, which indicates that

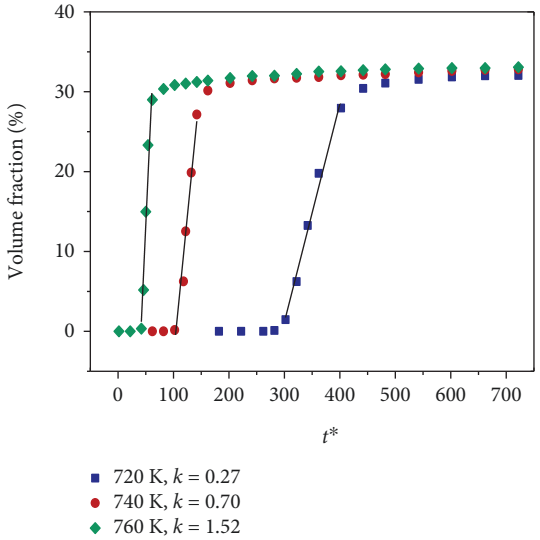

Figure 4: The volume fraction of the α' phase in the Fe-38 at.% Cr-10 at.% Al alloy as a function of time aged at 720, 740, and 760 K (solid lines represent the fitting of the volume fraction at the stage of initial phase separation).

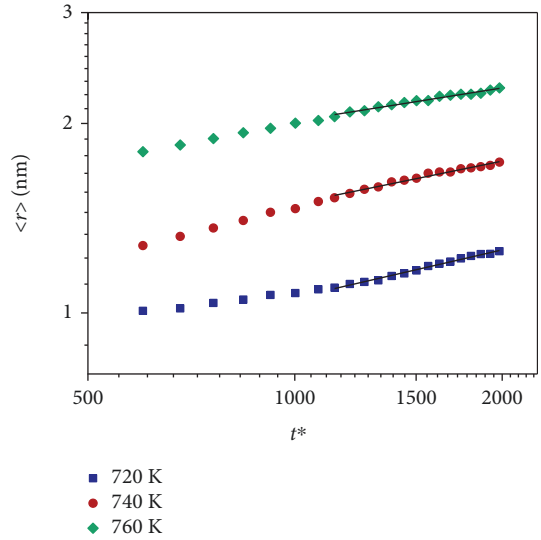

Figure 5: The average particle radius of the α' phase at a later coarsening stage in the Fe-38 at.% Cr-10 at.% Al alloy as a function of time aged at 720, 740, and 760 K.

the α' phase has not yet formed. The volume fraction starts to increase at $t^* = 42$ for 760 K, which means that the α' phase begins to separate. In comparison, the starting times for the separation of the α' phase are $t^* = 102$ and 282 at 740 and 720 K, respectively. Therefore, the higher the temperature is, the earlier the Cr-enriched phase appears, which indicates that the diffusion promotes the phase separation at high temperature, even if the supercooling is small, so the phase separation is a diffusion-controlled process in the range of 720 K to 760 K in the Fe-38 at.% Cr-10 at.% Al alloy.

At the stage of initial phase separation, the volume fraction increases quickly and the slopes k of the volume fraction are 0.27, 0.70, and 1.52 for the aging temperatures of 720, 740, and 760 K, respectively. This demonstrates again that the initial phase separation is faster for higher temperatures. The equilibrium value of 33% for the volume fraction is similar for different aging temperatures. However, the volume fraction in the low-Cr-concentration alloy, Fe-20 at.% Cr-10 at.% Al, aged at 748 K for 3600 h, does not reach equilibrium still, so an overlap of nucleation, growth, and coarsening is observed [22]. In the present Fe-38 at.% Cr-10 at.% Al alloy, a high Cr concentration enables achieving the equilibrium volume fraction early.

Figure 5 shows the evolution of the average particle radius $\langle r \rangle$ of the α' phase at a later coarsening stage in the Fe-38 at.% Cr-10 at.% Al alloy. Here, the average particle radius is calculated by $\langle r \rangle = \sqrt{S/\pi N}$, where S is the total area of the α' phase in two dimensions and N is the particle number of the α' phase. The average particle radius of the α' phase increases from 1.25 nm to 2.28 nm at $t^* = 1982$ for a temperature increasing from 720 K to 760 K. The size of the α' particles in the aged Fe-38 at.% Cr-10 at.% Al alloy is similar to that in binary Fe-Cr alloys. For example, Xu et al. showed that the radius of the α' particles are 0.96 nm and 2.04 nm after aging for 10 h and 100 h in the Fe-35 wt.% Cr alloy aged at 773 K [56]. The particle radius in the Fe-32 at.% Cr alloy aged at 743 K for 192-10000 h increases from 1.5 nm to 3.0 nm [57], and the average particle radius of the α' phase ranges from 0.95 nm to 2.53 nm in the Fe-20 at.% Cr alloy aged at 773 K for 50-1067 h [58].

At a later coarsening stage, the volume fractions reach equilibrium values, which means that the α' phase enters into the steady-state coarsening stage. The time exponents n of $\langle r \rangle \sim (t^*)^n$ for temperatures 720, 740, and 760 K at the coarsening stage are 0.25, 0.22, and 0.17, respectively. It should be noted that the time exponents are less than 1/3 predicated by the Lifshitz-Slyozov-Wagner (LSW) theory, in which a dilute solution without elastic interactions and with a very small volume fraction is assumed [59, 60]. Experimental results showed a time exponent of 0.25 in the Fe-30 at.% Cr alloy aged at 773 K [18], while the time exponent is 0.17 for the Fe-32 at.% Cr alloy aged at 773 K for 50 h [49]. In addition, there are some other experimental results showing that the coarsening time exponents are less than 1/3 [57, 61].

In order to show the changes in the coarsening rate of the α' phase with temperature, the cube of the average particle radius $\langle r \rangle^3$ and time t are fitted with the linear function for the Fe-38 at.% Cr-10 at.% Al alloy at the coarsening stage. The coarsening rate constants at 720, 740, and 760 K are $k_c = 8.06 \times 10^{-4}$, $k_c = 1.91 \times 10^{-3}$, and $k_c = 3.47 \times 10^{-3}$, respectively. It indicates that the coarsening rate constant increases with the increased aging temperature, which is attributed to the accelerated atomic mobility at high temperature [62].

As has been discussed in Figure 1, the coarsening of the α' phase can happen through the Ostwald ripening and coalescence coarsening of neighboring particles which are affected by the particles' distance. Therefore, the coarsening rate will be affected by the coarsening mechanism and

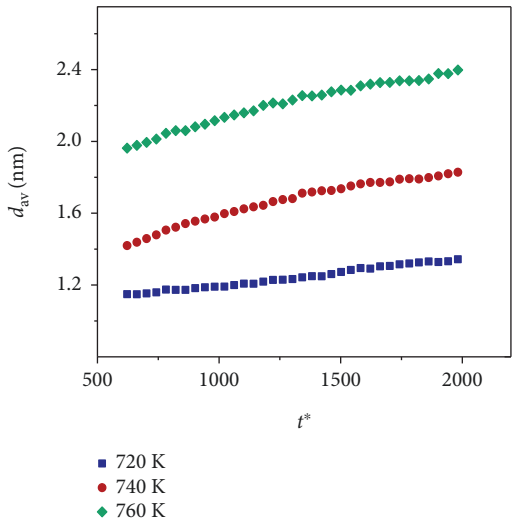

FIGURE 6: The average interparticle distance d_{av} of the α' phase in the Fe-38 at.% Cr-10 at.% Al alloy as a function of time when aged at 720, 740, and 760 K.

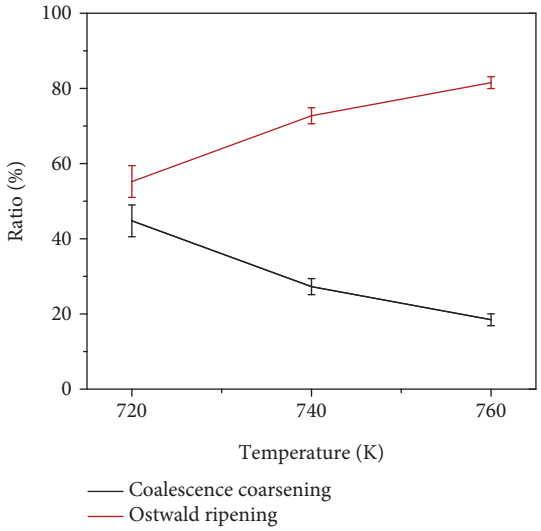

FIGURE 7: The ratio of the Ostwald ripening and coalescence coarsening for the coarsening of the α' phase in the Fe-38 at.% Cr-10 at.% Al alloy aged at 720, 740, and 760 K.

the particles' distance. We calculated the average interparticle distance d_{av} of the α' phase in the Fe-38 at.% Cr-10 at.% Al alloy aged at 720, 740, and 760 K, as shown in Figure 6. d_{av} is calculated as the average center-to-center distance of the two neighboring particles, $d_{av} = \sqrt{A/N} - \langle d \rangle$, where A is the total measured area and $\langle r \rangle$ is the average particle diameter of the α' phase. It is shown that the average interparticle distance increases with aging time and increasing temperature.

Then, the ratio of the Ostwald ripening and coalescence coarsening is calculated at the coarsening stage in the Fe-38 at.% Cr-10 at.% Al alloy, as shown in Figure 7. The average interparticle distance of the α' phase is the smallest for the aging temperature of 720 K, in which the ratio of coalescence

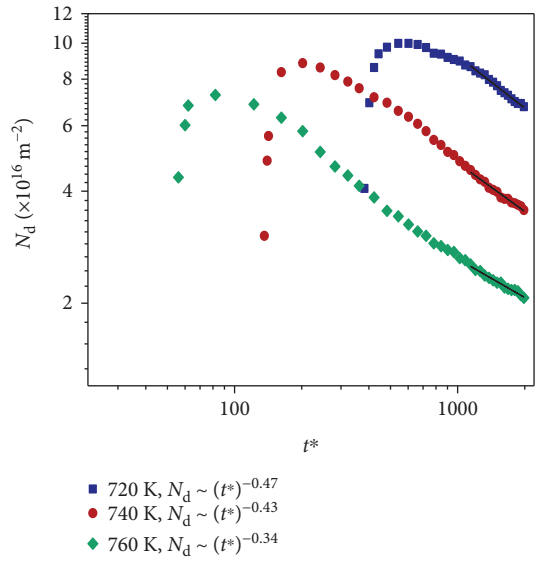

FIGURE 8: The particle number density N_d of the α' phase in the Fe-38 at.% Cr-10 at.% Al alloy as a function of time when aged at 720, 740, and 760 K (solid lines represent the fitting of particle number density at the later coarsening stage).

coarsening has a maximum of 44.78% among the three temperatures, while it is still less than the ratio of the Ostwald ripening of 55.22%. The ratio of 81.54% of the Ostwald ripening is the largest at 760 K. It is well known that the coarsening rate is larger in the way of Ostwald ripening than in the way of coalescence coarsening [63], and the ratio of the Ostwald ripening is greater than that of coalescence coarsening; therefore, the coarsening rate constant k_c of the α' phase increases with increased temperature at the coarsening stage in the Fe-38 at.% Cr-10 at.% Al alloy.

Figure 8 shows the particle number density N_d of the α' phase as a function of time for the Fe-38 at.% Cr-10 at.% Al alloy aged at 720, 740, and 760 K. The number density is calculated by the α' phase number per unit area. It can be seen that the particle number density increases at the early phase separation stage; when the maximum value is reached, it begins to decrease at $t^* = 602$, 202, and 82 for the aging temperatures of 720, 740, and 760 K, respectively, which means that the α' phase enters into the stage of coarsening earlier at 760 K than at the other temperatures. However, the maximum value of the particle number density at 760 K is the smallest of the three temperatures, and the maximum values of N_{dmax} are 9.99×10^{16} m^{-2}, 8.83×10^{16} m^{-2}, and 7.26×10^{16} m^{-2}, respectively, at 720, 740, and 760 K. This is because the supercooling is larger for a lower temperature and more particles are separated with a large driving force, which results in the maximum value of N_d at 720 K. The present N_d is similar to the previous simulations and experimental results. For example, N_{dmax} is 9.81×10^{16} m^{-2} in the Fe-35 at.% Cr alloy aged at 700 K [64], and the maximum value of N_d is also similar to the values obtained from the APT results [58].

The time exponents of the particle number density are calculated by fitting the relationship of $N_d \sim (t^*)^m$ at the coarsening stage. The time exponents m are -0.47, -0.43,

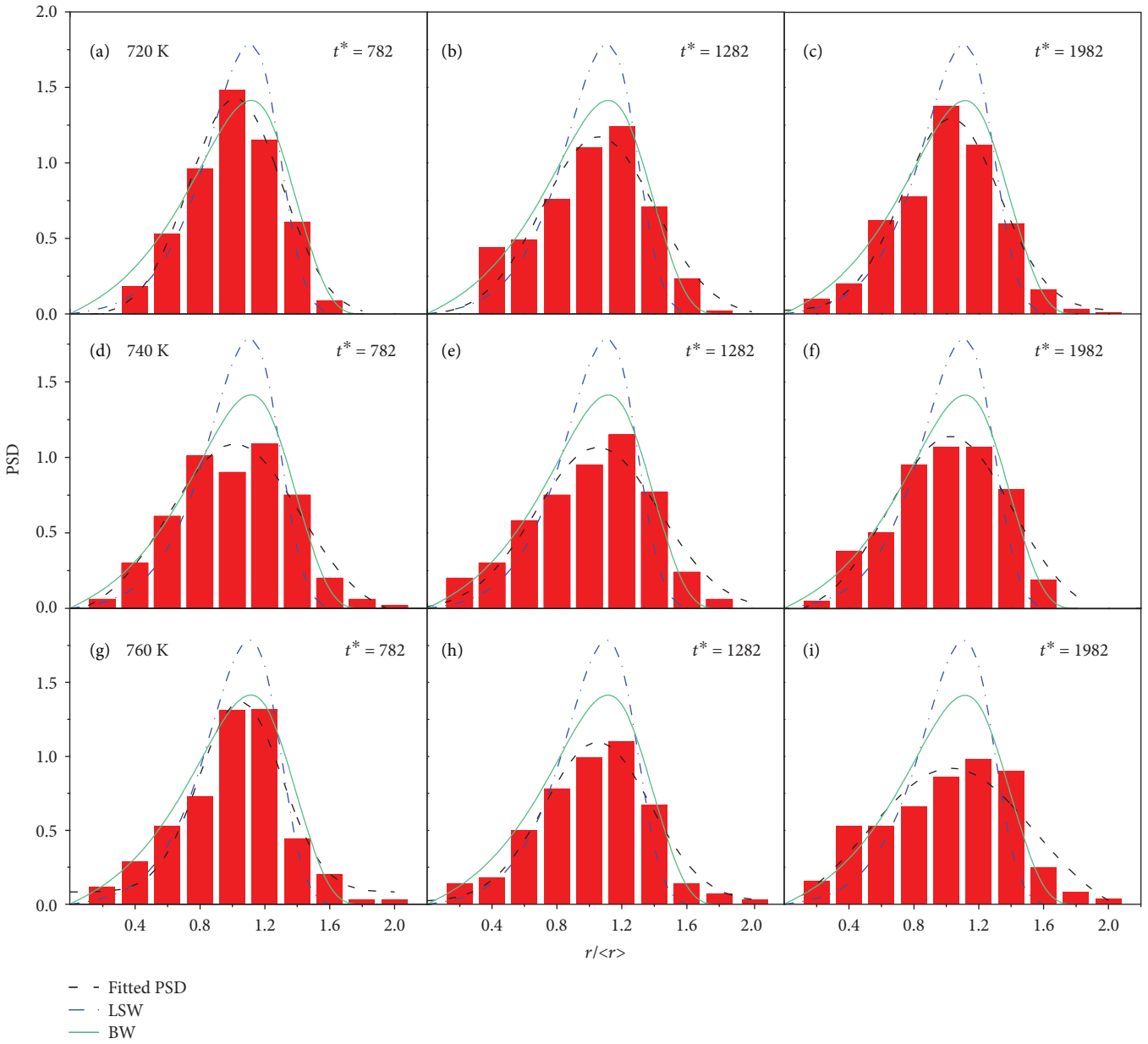

Figure 9: Particle size distribution of the α' phase in the Fe-38 at.% Cr-10 at.% Al alloy aged at 720, 740, and 760 K (dashed lines represent the Gaussian distribution of the histogram, dash-dot lines represent the LSW theory, and solid lines represent the BW model).

and -0.34 for the aging temperatures 720, 740, and 760 K, respectively. It is shown that the negative time exponents of the particle number density decrease with increased aging temperature, which is consistent with the time exponents of the average particle radius at the coarsening stage.

3.3. Particle Size Distribution of α' Phase. As shown in Figure 9, the histograms of the particle size distribution (PSD) of the α' phase aged at 720, 740, and 760 K are plotted by the distribution function $f(u)$. The x-axis represents the normalized particle radius $u = r/\langle r \rangle$, where r and $\langle r \rangle$ are the radius and average radius of the α' phase, respectively. The black dashed line is the Gaussian distribution of the histogram. Also plotted in Figure 9 are the PSD of the LSW theory [59, 60] illustrated with blue dash-dot lines and the PSD predicated by the Brailsford-Wynblatt (BW) model [65] illustrated with green solid lines. Both the LSW theory and the BW model are used to predicate particle size distribution. The equations of the BW model are referred from the literature [65]. The PSD of the LSW theory is calculated as follows [59, 60]:

$$\begin{cases} F_{\mathrm{LSW}} = \dfrac{81}{2^{5/3}} \times \dfrac{u^2}{(1.5-u)^{11/3}} \times \dfrac{1}{(3+u)^{7/3}} e^{-u/(1.5-u)}, & u < 1.5, \\ F_{\mathrm{LSW}} = 0, & u \geq 1.5, \end{cases} \tag{6}$$

It can be seen from Figure 9 that no matter at which aging temperature the peak value of the LSW theory is higher than that of the fitted PSD. The reason for this is that the LSW theory does not take into account the effect of the volume fraction and elastic interactions. Compared with the LSW theory, the fitted PSD is close to the curve of the BW model, especially at low temperature (Figures 9(a)–9(c)) and during the early phase separation stage (Figure 9(g)). We can find that the peak values of the fitted PSD decrease with the aging time at 760 K. However, the peak values of the PSD have no obvious changes at 720 and 740 K, which indicates that the higher aging temperature has a great impact on the size distribution of the α' phase. The peak positions of the fitted PSD are around $r/\langle r\rangle = 1.1$, which is similar to the 1.15 of the LSW and BW theory. It is found that the peak values of the PSD in the Fe-35 at.% Cr binary alloy decrease with time [48], and the peak positions at $r/\langle r\rangle = 1.1$ are the same as that of the Fe-38 at.% Cr-10 at.% Al alloy.

4. Conclusions

The morphology evolution, compositional partitioning, and separation kinetics of the nanoscale α' phase are investigated in the Fe-38 at.% Cr-10 at.% Al alloy aged at 720, 740, and 760 K by utilizing phase-field simulation. As the aging temperature increases, the phase separation, change of the composition, and volume fraction of the α' phase are faster, and the coarsening rate constant of the α' phase increases, which results in the large average radius of the α' particles at high temperature. Al depletes in the α' phase and partitions strongly into the Fe-enriched α phase. At the coarsening stage, the time exponents of the average particle radius of the α' phase decreases from 0.25 of 720 K to 0.17 of 760 K. Also, the negative time exponents of the particle number density of the α' phase decrease with increasing temperature. The coarsening of the α' phase happens via coalescence coarsening and the Ostwald ripening, and the Ostwald ripening is dominating at the coarsening stage with the enlarged average particle distance of the α' phase as the aging temperature increases. The peak values of the PSD decrease with the aging time at 760 K, while the width is broadened compared to that of 720 and 740 K. In addition, the PSD is close to the BW's distribution. The simulations show consistent results with the experiments and theoretical predications, while some questions need to be studied further for the high-throughput simulation, such as the composition-dependent gradient coefficients and the diffusion coefficients.

Data Availability

The data used to support the findings of this study are included within the article.

Conflicts of Interest

The authors declare that they have no conflicts of interest.

Acknowledgments

This work was supported by the National Natural Science Foundation of China (Grant Number 51571122) and the Fundamental Research Funds for the Central Universities (Grant Number 30916015107).

References

[1] J. Chao, C. Capdevila, M. Serrano, A. Garcia-Junceda, J. A. Jimenez, and M. K. Miller, "Effect of α-α' phase separation on notch impact behavior of oxide dispersion strengthened (ODS) Fe20Cr5Al alloy," *Materials & Design*, vol. 53, pp. 1037–1046, 2014.

[2] C. Capdevila, M. K. Miller, F. A. López, G. Pimentel, and J. Chao, "Reverse α-α' phase separation in Fe-20Cr-6Al alloy," *Philosophical Magazine*, vol. 93, no. 14, pp. 1640–1651, 2013.

[3] J. Ejenstam, M. Thuvander, P. Olsson, F. Rave, and P. Szakalos, "Microstructural stability of Fe-Cr-Al alloys at 450-550 °C," *Journal of Nuclear Materials*, vol. 457, pp. 291–297, 2015.

[4] Z. Foxman, O. Sobol, M. Pinkas et al., "Microstructural evolution of Cr-rich ODS steels as a function of heat treatment at 475 °C," *Metallography, Microstructure, and Analysis*, vol. 1, no. 3–4, pp. 158–164, 2012.

[5] K. G. Field, X. Hu, K. C. Littrell, Y. Yamamoto, and L. L. Snead, "Radiation tolerance of neutron-irradiated model Fe-Cr-Al alloys," *Journal of Nuclear Materials*, vol. 465, pp. 746–755, 2015.

[6] C. Capdevila, J. Chao, J. A. Jimenez, and M. K. Miller, "Effect of nanoscale precipitation on strengthening of ferritic ODS Fe-Cr-Al alloy," *Materials Science and Technology*, vol. 29, no. 10, pp. 1179–1184, 2013.

[7] S. A. Briggs, P. D. Edmondson, K. C. Littrell et al., "A combined APT and SANS investigation of α' phase precipitation in neutron-irradiated model FeCrAl alloys," *Acta Materialia*, vol. 129, pp. 217–228, 2017.

[8] S. Ukai, M. Harada, H. Okada et al., "Alloying design of oxide dispersion strengthened ferritic steel for long life FBRs core materials," *Journal of Nuclear Materials*, vol. 204, pp. 65–73, 1993.

[9] G. Bonny, D. Terentyev, and L. Malerba, "On the α-α' miscibility gap of Fe-Cr alloys," *Scripta Materialia*, vol. 59, no. 11, pp. 1193–1196, 2008.

[10] R. O. Williams and H. W. Paxton, "The nature of aging of binary iron-chromium alloys around 500 °C," *Journal of the Iron and Steel Institute*, vol. 185, pp. 358–374, 1957.

[11] J. Chao and J. L. González-Carrasco, "The influence of processing on the 475 °C hardening of MA 956 alloy," *Scripta Materialia*, vol. 47, no. 6, pp. 423–428, 2002.

[12] D. Chandra and L. H. Schwartz, "Mössbauer effect study of the 475 °C decomposition of Fe-Cr," *Metallurgical Transactions*, vol. 2, no. 2, pp. 511–519, 1971.

[13] W. Xiong, P. Hedström, M. Selleby, J. Odqvist, M. Thuvander, and Q. Chen, "An improved thermodynamic modeling of the Fe-Cr system down to zero Kelvin coupled with key experiments," *Calphad*, vol. 35, no. 3, pp. 355–366, 2011.

[14] K. G. Field, K. C. Littrell, and S. A. Briggs, "Precipitation of α' in neutron irradiated commercial FeCrAl alloys," *Scripta Materialia*, vol. 142, pp. 41–45, 2018.

[15] S. Kobayashi and T. Takasugi, "Mapping of 475 °C embrittlement in ferritic Fe-Cr-Al alloys," *Scripta Materialia*, vol. 63, no. 11, pp. 1104–1107, 2010.

[16] W. Xiong, M. Selleby, Q. Chen, J. Odqvist, and Y. Du, "Phase equilibria and thermodynamic properties in the Fe-Cr system," *Critical Reviews in Solid State and Materials Sciences*, vol. 35, no. 2, pp. 125–152, 2010.

[17] M. K. Miller, J. M. Hyde, M. G. Hetherington, A. Cerezo, G. D. W. Smith, and C. M. Elliott, "Spinodal decomposition in Fe-Cr alloys: experimental study at the atomic level and comparison with computer models—I. Introduction and methodology," *Acta Metallurgica et Materialia*, vol. 43, no. 9, pp. 3385–3401, 1995.

[18] J. M. Hyde, M. K. Miller, M. G. Hetherington, A. Cerezo, G. D. W. Smith, and C. M. Elliott, "Spinodal decomposition in Fe-Cr alloys: experimental study at the atomic level and comparison with computer models—II. Development of domain size and composition amplitude," *Acta Metallurgica et Materialia*, vol. 43, no. 9, pp. 3403–3413, 1995.

[19] J. Zhou, J. Odqvist, M. Thuvander, and P. Hedström, "Quantitative evaluation of spinodal decomposition in Fe-Cr by atom probe tomography and radial distribution function analysis," *Microscopy and Microanalysis*, vol. 19, no. 3, pp. 665–675, 2013.

[20] O. Senninger, E. Martínez, F. Soisson, M. Nastar, and Y. Bréchet, "Atomistic simulations of the decomposition kinetics in Fe-Cr alloys: influence of magnetism," *Acta Materialia*, vol. 73, pp. 97–106, 2014.

[21] Y. Li, L. Zhu, C. Liu, and S. Shi, "Nanoscale phase evolution during continuum decomposition of Fe-Cr alloys," *Materials*, vol. 10, no. 12, article 1431, 2017.

[22] C. Capdevila, M. K. Miller, and J. Chao, "Phase separation kinetics in a Fe-Cr-Al alloy," *Acta Materialia*, vol. 60, no. 12, pp. 4673–4684, 2012.

[23] W. Li, S. Lu, Q. M. Hu, H. Mao, B. Johansson, and L. Vitos, "The effect of Al on the 475 °C embrittlement of Fe-Cr alloys," *Computational Materials Science*, vol. 74, pp. 101–106, 2013.

[24] Y. Suwa and Y. Saito, "Effect of Mo on phase separation in Fe-40 at% Cr alloys based on numerical solutions of the Cahn Hilliard equation," *Materials Transactions*, vol. 48, no. 7, pp. 1891–1895, 2007.

[25] Y. Suwa, Y. Saito, K. Ochi, T. Aoki, K. Goto, and K. Abe, "Kinetics of phase separation in Fe-Cr-Mo ternary alloys," *Materials Transactions*, vol. 43, no. 2, pp. 271–276, 2002.

[26] L. X. Lv, L. Zhen, C. Y. Xu, and X. Y. Sun, "Phase field simulation of microstructure evolution in Fe-Cr-Co alloy during thermal magnetic treatment and step aging," *Journal of Magnetism and Magnetic Materials*, vol. 322, no. 8, pp. 987–995, 2010.

[27] N. Moelans, B. Blanpain, and P. Wollants, "An introduction to phase-field modeling of microstructure evolution," *Calphad*, vol. 32, no. 2, pp. 268–294, 2008.

[28] J. W. Cahn and J. E. Hilliard, "Free energy of a nonuniform system. I. Interfacial free energy," *The Journal of Chemical Physics*, vol. 28, no. 2, pp. 258–267, 1958.

[29] K. Wu, J. E. Morral, and Y. Wang, "Movement of Kirkendall markers, second phase particles and the type 0 boundary in two-phase diffusion couple simulations," *Acta Materialia*, vol. 52, no. 7, pp. 1917–1925, 2004.

[30] K. Wu, J. E. Morral, and Y. Wang, "A phase field study of microstructural changes due to the Kirkendall effect in two-phase diffusion couples," *Acta Materialia*, vol. 49, no. 17, pp. 3401–3408, 2001.

[31] C. Huang, M. O. de la Cruz, and B. W. Swift, "Phase separation of ternary mixtures: symmetric polymer blends," *Macromolecules*, vol. 28, no. 24, pp. 7996–8005, 1995.

[32] Japan Institute of Metals, *Metals Data Book*, Maruzen, Tokyo, 1993.

[33] T. Koyama and H. Onodera, "Modeling of microstructure changes in Fe-Cr-Co magnetic alloy using the phase-field method," *Journal of Phase Equilibria and Diffusion*, vol. 27, no. 1, pp. 22–29, 2006.

[34] G. E. Dieter, *Mechanical Metallurgy*, McGraw-Hill, London, 1988.

[35] A. Heesemann, E. Schmidtke, F. Faupel, A. Kolb-Telieps, and J. Klöwer, "Aluminum and silicon diffusion in Fe-Cr-Al alloys," *Scripta Materialia*, vol. 40, no. 5, pp. 517–522, 1999.

[36] R. R. Mohanty and Y. Sohn, "Phase-field investigation of multicomponent diffusion in single-phase and two-phase diffusion couples," *Journal of Phase Equilibria and Diffusion*, vol. 27, no. 6, pp. 676–683, 2006.

[37] J. W. Cahn, "Phase separation by spinodal decomposition in isotropic systems," *The Journal of Chemical Physics*, vol. 42, no. 1, pp. 93–99, 1965.

[38] J. O. Andersson and B. Sundman, "Thermodynamic properties of the Cr-Fe system," *Calphad*, vol. 11, no. 1, pp. 83–92, 1987.

[39] T. Minowa, M. Okada, and M. Homma, "Further studies of the miscibility gap in an Fe-Cr-Co permanent magnet system," *IEEE Transactions on Magnetics*, vol. 16, no. 3, pp. 529–533, 1980.

[40] A. T. Dinsdale, "SGTE data for pure elements," *Calphad*, vol. 15, no. 4, pp. 317–425, 1991.

[41] M. H. G. Jacobs, R. Schmid-Fetzer, T. Markus, V. Motalov, G. Borchardt, and K. H. Spitzer, "Thermodynamics and diffusion in ternary Fe-Al-Cr alloys, part I: thermodynamic modeling," *Intermetallics*, vol. 16, no. 8, pp. 995–1005, 2008.

[42] D. Rohrberg, K. H. Spitzer, L. Dörrer et al., "Host atom diffusion in ternary Fe-Cr-Al alloys," *Metallurgical and Materials Transactions A*, vol. 45, no. 1, pp. 269–279, 2014.

[43] M. Hillert and M. Jarl, "A model for alloying in ferromagnetic metals," *Calphad*, vol. 2, no. 3, pp. 227–238, 1978.

[44] E. A. Lass, W. C. Johnson, and G. J. Shiflet, "Correlation between CALPHAD data and the Cahn-Hilliard gradient energy coefficient and κ exploration into its composition dependence," *Calphad*, vol. 30, no. 1, pp. 42–52, 2006.

[45] E. A. Brandes and G. B. Brook, *Smithells Metals Reference Book*, ASM, International, eighth ed. edition, 2004.

[46] L. Q. Chen and J. Shen, "Applications of semi-implicit Fourier-spectral method to phase field equations," *Computer Physics Communications*, vol. 108, no. 2–3, pp. 147–158, 1998.

[47] C. Capdevila, M. K. Miller, K. F. Russell, J. Chao, and J. L. González-Carrasco, "Phase separation in PM 2000™ Fe-base ODS alloy: experimental study at the atomic level," *Materials Science and Engineering: A*, vol. 490, no. 1–2, pp. 277–288, 2008.

[48] Z. Yan, Y. Li, X. Zhou, Y. Zhang, and R. Hu, "Evolution of nanoscale Cr-rich phase in a Fe-35 at.% Cr alloy during isothermal aging," *Journal of Alloys and Compounds*, vol. 725, no. 25, pp. 1035–1043, 2017.

[49] O. Soriano-Vargas, E. O. Avila-Davila, V. M. Lopez-Hirata, N. Cayetano-Castro, and J. L. Gonzalez-Velazquez, "Effect of

spinodal decomposition on the mechanical behavior of Fe-Cr alloys," *Materials Science and Engineering: A*, vol. 527, no. 12, pp. 2910–2914, 2010.

[50] V. M. Lopez-Hirata, O. Soriano-Vargas, H. J. Rosales-Dorantes, and M. L. S. Muñoz, "Phase decomposition in an Fe-40 at.% Cr alloy after isothermal aging and its effect on hardening," *Materials Characterization*, vol. 62, no. 8, pp. 789–792, 2011.

[51] H. G. Read and K. Hono, "Phase-separation, partitioning and precipitation in MA956, an ODS ferritic stainless steel," *Le Journal de Physique IV*, vol. 6, no. C5, pp. C5-223–C5-228, 1996.

[52] C. Capdevila, M. K. Miller, and K. F. Russell, "Aluminum partitioning during phase separation in Fe-20%Cr-6%Al ODS alloy," *Journal of Materials Science*, vol. 43, no. 11, pp. 3889–3893, 2008.

[53] H. G. Read, H. Murakami, and K. Hono, "Al partitioning in MA 956, an ODS ferritic stainless steel," *Scripta Materialia*, vol. 36, no. 3, pp. 355–361, 1997.

[54] E. Airiskallio, E. Nurmi, M. H. Heinonen et al., "High temperature oxidation of Fe-Al and Fe-Cr-Al alloys: the role of Cr as a chemically active element," *Corrosion Science*, vol. 52, no. 10, pp. 3394–3404, 2010.

[55] C. Capdevila, M. M. Aranda, R. Rementeria et al., "Strengthening by intermetallic nanoprecipitation in Fe-Cr-Al-Ti alloy," *Acta Materialia*, vol. 107, no. 1, pp. 27–37, 2016.

[56] X. Xu, J. Odqvist, M. H. Colliander et al., "Structural characterization of phase separation in Fe-Cr: a current comparison of experimental methods," *Metallurgical and Materials Transactions A*, vol. 47, no. 12, pp. 5942–5952, 2016.

[57] S. S. Brenner, M. K. Miller, and W. A. Soffa, "Spinodal decomposition of iron-32 at.% chromium at 470 °C," *Scripta Metallurgica*, vol. 16, no. 7, pp. 831–836, 1982.

[58] S. Novy, P. Pareige, and C. Pareige, "Atomic scale analysis and phase separation understanding in a thermally aged Fe-20 at.%Cr alloy," *Journal of Nuclear Materials*, vol. 384, no. 2, pp. 96–102, 2009.

[59] I. M. Lifshitz and V. V. Slyozov, "The kinetics of precipitation from supersaturated solid solutions," *Journal of Physics and Chemistry of Solids*, vol. 19, no. 1–2, pp. 35–50, 1961.

[60] C. Wagner, "Theorie der alterung von niederschlägen durch umlösen (Ostwald-reifung)," *Zeitschrift für Elektrochemie, Berichte der Bunsengesellschaft für physikalische Chemie*, vol. 65, no. 7-8, pp. 581–591, 1961.

[61] F. Bley, "Neutron small-angle scattering study of unmixing in Fe-Cr alloys," *Acta Metallurgica et Materialia*, vol. 40, no. 7, pp. 1505–1517, 1992.

[62] A. V. Danilychev and V. A. Apkarian, "Temperature induced mobility and recombination of atomic oxygen in crystalline Kr and Xe. I. Experiment," *The Journal of Chemical Physics*, vol. 99, no. 11, pp. 8617–8627, 1993.

[63] Z. Mao, C. K. Sudbrack, K. E. Yoon, G. Martin, and D. N. Seidman, "The mechanism of morphogenesis in a phase-separating concentrated multicomponent alloy," *Nature Materials*, vol. 6, no. 3, pp. 210–216, 2007.

[64] Y. Li, Z. Yan, and X. Zhou, "Kinetics of initial phase separation and coarsening of nanoscale phase in Fe-Cr alloys," *Journal of Nuclear Materials*, vol. 497, pp. 154–160, 2017.

[65] A. D. Brailsford and P. Wynblatt, "The dependence of Ostwald ripening kinetics on particle volume fraction," *Acta Metallurgica*, vol. 27, no. 3, pp. 489–497, 1979.